

## Using nitroxide spin labels

### How to obtain $T_{1e}$ from continuous wave electron paramagnetic resonance spectra at all rotational rates

D. A. Haas, C. Mailer, and B. H. Robinson

Chemistry Department, University of Washington, Seattle, Washington 98195 USA

**ABSTRACT** Historically, the continuous wave electron paramagnetic resonance (CW-EPR) progressive saturation method has been used to obtain information on the spin-lattice relaxation time ( $T_{1e}$ ) and those processes, such as motion and spin exchange, that occur on a competitive timescale. For example, qualitative information on local dynamics and solvent accessibility of proteins and nucleic acids has been obtained by this method. However, making quantitative estimates of  $T_{1e}$  from CW-EPR spectra have been frustrated by a lack of understanding of the role of  $T_{1e}$  (and  $T_{2e}$ ) in the slow-motion regime. Theoretical simulation of the CW-EPR lineshapes in the slow-motion region under increasing power levels has been used in this work to test whether the saturation technique can produce *quantitative* estimates of the spin-lattice relaxation rates. A method is presented by which the correct  $T_{1e}$  may be extracted from an analysis of the power-saturation rollover curve, regardless of the amount of inhomogeneous broadening or the rates of molecular reorientation. The range of motional correlation times from 10 to 200 ns should be optimal for extracting quantitative estimates of  $T_{1e}$  values in spin-labeled biomolecules. The progressive-saturation rollover curve method should find wide application in those areas of biophysics where information on molecular interactions and solvent exposure as well as molecular reorientation rates are desired.

#### INTRODUCTION

The aim of this article is to determine whether the power saturation method of continuous wave electron paramagnetic resonance (CW-EPR) can be used to determine relaxation times of nitroxide spin labels. In the fast-motion limit where the EPR lines are homogeneously broadened, the standard saturation theory used to obtain  $T_{1e}$  and  $T_{2e}$  is well known and simple to apply (1, 2). However, as the motion slows the lines become inhomogeneously broadened because anisotropies in the  $g$ - and  $A$ -tensors are no longer completely averaged away, and the simple theory breaks down. A large body of work exists to analyze inhomogeneous lineshapes, primarily in the EPR of solids. To the best of our knowledge, virtually all previous work assumes some form of distribution of the individual, homogeneous resonance lines that is static on the time scale of the EPR measurement (3–5). Some treatments do allow spin diffusion (6, 7) but still assume Gaussian or Lorentzian line shapes. Freed and co-workers (8, 9) have studied saturation in liquids and demonstrated the line broadening effects of high microwave powers. The present treatment extends previous theoretical developments to show how a saturation curve may be used to obtain  $T_{1e}$  in an experimental situation.

The primary motivation for this article lies in the recent work of Altenbach et al. (10), who used changes in the apparent relaxation rates of spin labels to determine molecular structure. A label at a known position in a molecule that has some contact with a spin relaxing agent will have a faster relaxation rate compared with a control with no such relaxing agent. Relaxation rates

were not measured directly, but were obtained by CW power saturation of the first-derivative EPR signal. The CW-EPR signal height, when measured as a function of incident microwave power, rises to a maximum and then decreases. The incident power level at which the signal is reduced by 3 dB is called the “half-power” saturation parameter,  $P_{1/2}$ , and Altenbach et al. (10) used this quantity as a measure of the relaxation rate. Altenbach et al. determined the  $\alpha$ -helical nature of a *trans*-membrane protein from the periodicity of the  $P_{1/2}$  of a spin label selectively attached to a single amino acid side-chain in the sequence. The spin label relaxation rate increased for those amino acids that were in contact with an oxygen-rich lipid environment.

One assumption in simple theories of the relation between  $P_{1/2}$  and the relaxation rate is that the line measured is a single, homogeneous one. In general, the spectral lines are very definitely not homogeneous, being a complex mixture of partially averaged tensors and dynamical interactions, because the labels are moving in the nanosecond motional region. Nevertheless, the relative changes in  $P_{1/2}$  produced a plausible map of lipid accessibility. We wish to understand why the saturation method worked as well as it did and to determine whether there are any improvements that can be made in the methodology of the experiments. In particular, we wish to know whether the true spin-lattice relaxation time (in agreement with that measured by saturation recovery EPR) and the true spin-spin relaxation time can be obtained from power saturation studies when the motion is in the nanosecond regime. To do this we have computed EPR spectra of an  $^{14}\text{N}$  spin label over a wide range of microwave powers at various rotational correlation times and have analyzed the results. There are no assumptions about the distribution function of the inho-

Address correspondence to Dr. Bruce H. Robinson, Department of Chemistry, Room BG-10, University of Washington, Seattle, WA 98195, USA.

mogeneous broadening. The EPR simulation programs developed by us (11, 12) (originally for saturation transfer [ST]-EPR) explicitly include the  $A$ - and  $g$ -tensors, motion, the Zeeman modulation frequency, and the relaxation times.

## THEORY

The spectra were calculated by solving the spin density matrix equation that explicitly includes rf field levels, relaxation times, Zeeman modulation, and the correlation time for isotropic rotational Brownian motion of the label (11, 12). The equation of motion of the density matrix is:

$$\dot{\sigma}(\Omega, t) = -i[H(\Omega, t), \sigma(\Omega, t)] - \Gamma_R \{ \sigma(\Omega, t) - \sigma^0(\Omega, t) \} - \Gamma_\Omega \{ \sigma(\Omega, t) - \sigma^0(\Omega, t) \}, \quad (1)$$

where  $\sigma(\Omega, t)$  is the spin density matrix,  $H(\Omega, t)$  is the spin Hamiltonian, and  $\Gamma_\Omega$  is a Markoffian motional operator affecting only the orientation variable  $\Omega$ .  $\Gamma_R$  describes spin relaxation arising from the modulation of spatial coordinates other than  $\Omega$ , via a phenomenological fast-motion or Redfield type matrix, and includes  $T_{1e}$  and  $T_{2e}^0$  (13)—entered directly into the program—and  $\sigma^0(\Omega, t)$ , the equilibrium density matrix.<sup>1</sup> The Hamiltonian  $H(\Omega, t)$  may be expressed as:

$$H(\Omega, t) = \mathcal{H}_0 + \mathcal{H}_1(\Omega) + \epsilon(t),$$

where the orientation-independent Hamiltonian is given by:

$$\mathcal{H}_0 = \gamma_e H_0 S_z - \gamma_n H_0 I_z + \gamma_e \bar{a} [S_z I_z], \quad (2)$$

including isotropic electron Zeeman, nuclear Zeeman, and electron-nuclear hyperfine interactions.  $\gamma_e$  and  $\gamma_n$  are the electron and nuclear gyromagnetic ratios,  $H_0$  is the DC Zeeman field and  $\bar{a}$  is the isotropic hyperfine interaction.  $\mathcal{H}_1(\Omega)$  is the time-independent but orientation-dependent Hamiltonian and is given in detail elsewhere (11).  $\mathcal{H}_1(\Omega)$  is dependent on the anisotropies of the  $A$  (the electron-nuclear hyperfine) and  $g$  (the electron Zeeman) tensors as well as the rotation angles,  $\Omega$ , written in terms of the Wigner rotational matrix elements. The principal axes of the  $A$ - and  $g$ -tensors are assumed to be coincident.  $\mathcal{H}_1(\Omega)$  modifies the resonance position due to the orientation of the molecule, and it is this term that gives rise to asymmetries in the spectra when the motion is slow. When the motion is fast enough to average each manifold to a single line, then  $\mathcal{H}_1(\Omega)$  and  $\Gamma_\Omega$  may be removed from Eq. 1 and used to

compute the linewidth by fast-motion (Redfield) theory. The relaxation rate and time, predicted by fast-motion theory (13), are  $R_{2e}^G(m) = [T_{2e}^G(m)]^{-1}$ . The contribution of  $\mathcal{H}_1(\Omega)$  to the linewidth may be estimated as:

$$R_{2e}^G(m) \langle S_+ \rangle = \int_0^\infty \langle |[\mathcal{H}_1(\Omega)^x, [\mathcal{H}_1(\Omega), S_+]]| \rangle dt, \quad (3)$$

where  $\mathcal{H}_1(\Omega)$  in the rotating frame is:

$$\mathcal{H}_1(\Omega)^x = e^{-i\mathcal{H}_0 t} \mathcal{H}_1(\Omega) e^{+i\mathcal{H}_0 t}.$$

The equation for the relaxation rate predicted from simple fast-motion theory is given by Goldman et al. (14) (see Appendix). The total linewidth in the absence of inhomogeneous broadening is then predicted to be:

$$R_{2e}(m) = [T_{2e}(m)]^{-1} = R_{2e}^G(m) + [T_{2e}^0]^{-1}, \quad (4)$$

where an additional contribution to relaxation is specified only by  $T_{2e}^0$  (13). Eq. 4 is valid for  $m = 0$  or  $\pm 1$  for the  $^{14}\text{N}$  and  $m = \pm 1/2$  for the  $^{15}\text{N}$  spin label.

The time-dependent but orientation-independent Hamiltonian  $\epsilon(t)$  describes the interaction of the spins with the rf radiation and the low frequency modulation of the DC field:

$$\epsilon(t) = d_0 (S_+ e^{-i\omega_0 t} + S_- e^{+i\omega_0 t}) + d_m S_z (e^{-i\omega_m t} + e^{+i\omega_m t}),$$

where  $\omega_0$  and  $\omega_m$  are the frequencies of the microwave observing field of amplitude  $h_1$  and Zeeman modulation field, of amplitude  $h_m$ , respectively.  $d_0 = \frac{1}{2}\gamma_e h_1$  and  $d_m = \frac{1}{2}\gamma_e h_m$  are in frequency units. The matrix elements of  $\sigma$  are computed using the eigenfunctions of  $\mathcal{H}_0$  as a basis set. The observed signal is the deviation from equilibrium,  $\chi = \sigma - \sigma^0$  (11). In the high-field and high-temperature approximation the equilibrium spin density matrix is:

$$\sigma^0 = \{N^{-1} - q[\mathcal{H}_0 + \mathcal{H}_1(\Omega)]\} P^0(\Omega),$$

and  $q = \hbar / NkT$ ,  $P^0(\Omega)$  is the equilibrium orientation distribution (assumed isotropic) and  $N$  is the number of spin states (six for  $^{14}\text{N}$  and four for  $^{15}\text{N}$ ). These equations were programmed and solved for  $^{14}\text{N}$  spin labels on a DEC workstation (12). Note that all of the terms in the above equations used to calculate the CW-EPR spectra are, of necessity, stationary in the rotating frame. This means that none of the terms can generate a relaxation process for  $T_{1e}$  (terms that are nonstationary in the rotating frame are needed to produce a  $T_{1e}$ ).  $T_{1e}$  therefore is added into the equations via the phenomenological Redfield relaxation matrix,  $\Gamma_R$ , in Eq. 1.

## LINESHAPE ANALYSIS

The conventional CW-EPR experiment detects the absorption signal,  $M_y^1$ , at the first harmonic of the low frequency modulation frequency. In the picosecond corre-

<sup>1</sup>  $T_{2e}^0$  is the contribution to the linewidth from mechanisms not specified in the Hamiltonian. In this case it may arise from rapid fluctuations of the non-secular terms. It may be thought of as the intrinsic linewidth of the powder pattern in the absence of rotational motion. For spin labels one typically finds  $20 < T_{2e}^0 < 150$  ns.

lation time fast-motion limit  $^{14}\text{N}$  spin label absorption spectra consist of three narrow lines, whose amplitudes are given by (2):

$$M_y^1 = q\gamma_e h_m h_1 \left\{ \frac{2\Delta/T_{2e}}{(\Delta^2 + 1/S_0 T_{2e}^2)(\Delta^2 + 1/S_1 T_{2e}^2)} \right\}, \quad (5)$$

where

$$S_r = \left( 1 + \frac{(\gamma_e h_1)^2 T_{2e} T_{1e}}{1 + (r T_{1e} \omega_m)^2} \right)^{-1}, \quad (6)$$

and  $r = 0, 1, 2, 3 \dots$  is an index that refers to the harmonic of the modulation;  $\Delta$  is the frequency offset from the center of resonance. In the very fast-motion limit (picosecond correlation times), the spin-spin relaxation time is  $T_{2e}^0$ . As the motion slows,  $T_{2e}^0$  is replaced by the  $T_{2e}(m)$  given in Eq. 4. When  $\omega_m T_{1e} \ll 1$ , then  $S_1 \approx S_0$  and  $S_0 = \{1 + (\gamma_e h_1)^2 T_{2e} T_{1e}\}^{-1}$ , which is the usual saturation parameter (1).<sup>2</sup> In this situation, the equation reduces to the familiar derivative of a Lorentzian line:

$$M_y^1 = q\gamma_e h_m h_1 \left\{ \frac{2\Delta/T_{2e}}{(\Delta^2 + 1/S_0 T_{2e}^2)^2} \right\}. \quad (7)$$

The values of  $\Delta$  at which the peaks of the derivative occur are at  $\Delta_{\max} = \pm 1/(T_{2e}\sqrt{3S_0})$ . The peak-to-peak width of the line in gauss,  $L$ , is given by:

$$L^2 = L_0^2 + \frac{4}{3} h_1^2 \left( \frac{T_{1e}}{T_{2e}} \right), \quad (8)$$

where  $L_0$  is the peak-to-peak width in the limit of very low microwave field, i.e.,  $L_0 = 2/(\sqrt{3}T_{2e}\gamma_e)$ . Defining  $\Delta Y$  as the base-to-peak height of  $M_y^1$  and substituting the values of  $\Delta_{\max}$  into Eq. 7 for  $M_y^1$  gives:

$$\Delta Y = 0.7 \times q\gamma_e h_m h_1 T_{2e}^2 S_0^{3/2}.$$

At low powers,  $S_0$  is approximately unity and the signal is proportional to  $h_1$ . As  $h_1$  increases,  $S_0$  decreases, and the signal levels off. At still higher levels of  $h_1$ , the term in  $S_0$  dominates and the signal decreases, eventually becoming proportional to  $1/h_1^2$ . The peak-to-peak height will be maximized when  $h_1 = 1/\sqrt{2\gamma_e^2 T_{1e} T_{2e}}$  and  $S_0 = 2/3$ . The experimental variable is the microwave power incident on the sample,  $P_0$ , and this is related to  $h_1$  by the equation  $h_1 = \alpha\sqrt{P_0}$ , where  $\alpha$  is the power to rf field conversion factor that is a function of the resonator and sample used. The relation of signal to microwave power is now in the standard form (1, 2, 15):

$$\Delta Y = \frac{cP_0^{1/2}}{(1 + P_0/P_2)^\epsilon}, \quad (9)$$

where  $c$  is an (adjustable) gain constant, and  $\epsilon$  is a parameter to take account of the lineshape:  $\epsilon = 3/2$  for a homoge-

neous first-derivative absorption line, is unity for a zero derivative absorption line (3), and is  $1/2$  for a completely inhomogeneous derivative absorption line.  $P_2$  is a saturation parameter (in units of Watts) and is defined as:

$$P_2 = [(\gamma_e \alpha)^2 T_{1e} T_{2e}]^{-1}. \quad (10)$$

Eqs. 9 and 10 are central to the analysis to obtain  $T_{1e} - P_2$  is obtained from Eq. 9 and  $T_{1e}$  is calculated from Eq. 10, provided an estimate of  $T_{2e}$  can be obtained. It is the correct value of  $T_{2e}$  to use that has been the major problem in previous analyses. If the EPR lines are pure Lorentzians, then  $T_{2e}$  is easily found from the linewidth; most experimental spectra have much more complicated lineshapes, and the correct  $T_{2e}$  value is not obvious. We believe that this situation can be solved by combining the  $\epsilon$  parameter of Eq. 9 with a linewidth measured from the spectrum to obtain an estimate of the correct " $T_{2e}$ " to use in Eq. 10. The next few paragraphs justify the use of  $\epsilon$  in this endeavor.

Fig. 1 shows the shape of the line at the low field turning point of the first harmonic EPR spectrum. It is anticipated that the saturation characteristics of this low field turning point should be those of a first harmonic (or first-derivative) Lorentzian absorption line ( $\epsilon = 3/2$ ). When in the fast-motion limit (Fig. 1, top) and approximately those of a zeroth-derivative Lorentzian absorption line ( $\epsilon = 1$ ) in the near no-motion limit (Fig. 1, bottom). To go smoothly from the fast-motion limit to the slow-motion limit, it seems reasonable therefore that we let  $\epsilon$  be an adjustable parameter. Often the maximum of the rolover curve,  $P_{\max}$ , is of interest. From Eq. 9 it follows that  $P_{\max} = P_2/(2\epsilon - 1)$ . The  $P_{1/2}$  parameter used by Altenbach et al. (10) is defined as the intersection of a straight line  $\Delta Y_0 = (c/2)P_0^{1/2}$ , with the curve defined by Eq. 9. The intersection of these two lines occurs when  $P_{1/2} = P_2(2^{1/\epsilon} - 1)$ . For the special case of a pure absorption line where  $\epsilon = 1$ , then  $P_{1/2} = P_{\max} = P_2$ , but otherwise the three quantities are all slightly different. We consider  $P_2$  to be the preferred parameter for analysis because it is independent of  $\epsilon$ ;  $P_{\max}$  and  $P_{1/2}$  clearly depend on  $\epsilon$ .

Protons (or deuterons) surrounding the spin label N-O moiety cause unresolved broadening. To account for this effect, the calculated spectra were convolved with a Gaussian function and subsequently analyzed with Eq. 9. The value of  $\epsilon$  is influenced by the degree of homogeneity of the EPR line (15). Its value ranges from  $3/2$  for a single homogeneous line to  $1/2$  for a completely inhomogeneous line. The amount of broadening for protons (deuterons) is around 0.5 (0.17) G in the fast-motion limit and around 2.8 (0.9) G in the slow motion limit (16). The nonbroadened simulated lines had width  $< 1$  G at the fast-motion limit and several gauss in the slow motion limit, hence we expect  $\epsilon$  to be changed when we perform the convolution.

<sup>2</sup> Poole provides the definition of the  $S_0$  parameter on p. 590 of (1).

**TABLE 1** The  $A$  and  $g$ -tensors and the three relative turning points for each nuclear manifold

	$X$	$Y$	$Z$
$A$	6	6	31
$g$	2.0086	2.0066	2.0032
$m = -1$	1.76	5.15	35.91
$m = 0$	-4.24	-0.85	4.91
$m = +1$	-10.24	-6.85	-26.09

$m = +1$  (low field),  $m = 0$  (center field),  $m = -1$  (high field).  $A$ -tensor elements and turning points are in gauss.

It is our aim to show that Eq. 9 for the saturation rollover curve is robust enough to give a good accounting of the power dependence of the EPR signal regardless of the correlation time or the amount of proton (or deuteron) broadening. Changes in the shape of the saturation curve show up as changes in the values of  $\epsilon$  and  $P_2$ .

A way to roughly estimate  $1/T_{2e}$  from the spectrum, regardless of the motional rate, would be to use the width at half-peak height,  $W$ , on the tail of the Lorentzian (see Fig. 1). For a Lorentzian first harmonic (or derivative) spectrum with  $\epsilon = 3/2$ , we find that  $W = 0.809/\gamma_e T_{2e} \cong 1/\sqrt{\epsilon}\gamma_e T_{2e}$ . The zeroth-derivative absorption Lorentzian ( $\epsilon = 1.0$ ) yields  $W = 1/\gamma_e T_{2e}$ .  $R_w \equiv 1/T_{2e}$  is an effective linewidth that takes into account the lineshape changes that occur as the motional rate changes, and is defined as:

$$R_w = 1/T_{2e} \approx \sqrt{\epsilon}\gamma_e W, \quad (11)$$

where  $W$  is obtained when  $h_1$  is so small that no saturation is present.

Under saturation conditions, lines broaden, and Eq. 8 shows how the line width,  $L$ , depends on the observer amplitude. A linear plot of  $L^2$  vs.  $h_1^2$  has been used as a means of calibrating  $h_1$  (17) and can give  $T_{1e}$  provided  $T_{2e}$  is known. This method works well at fast motions typical of the spectra in Fig. 1 (*top*) and could, in principle, be used to analyze the data at slower correlation times (2). However, it failed in practice because the plots were nonlinear. Furthermore, there was no parameter analogous to  $\epsilon$  that could take account of shape changes in a simple way.

## METHODS

(a) The EPR spectra were simulated for different values of the incident observer amplitude,  $h_1$ , with a fixed set of parameters. Table 1 presents the  $A$ - and  $g$ -tensors used in all of the simulations, as well as the  $x$ ,  $y$ , and  $z$  turning points for each manifold,  $m = 0, \pm 1$ . The values of  $T_{1e}$  and  $T_{2e}^0$ , and the isotropic, Brownian rotational reorientation with characteristic correlation time,  $\tau_c$ , are in Table 2. The spectra were convolved with a Gaussian function to include the effects of protons (see Table 3).

(b) For a fixed set of parameters, a signal versus power rollover curve was obtained (see Fig. 2) and was fit by least-squares to a linearized version of Eq. 9:

$$[\Delta Y(P_0^{(\epsilon-1/2)})]^{1/\epsilon} = (c^{1/\epsilon} P_2) - P_2 \times [\Delta Y/P_0^{1/2}]^{1/\epsilon}, \quad (12)$$

to obtain  $c$  (which is of no interest),  $\epsilon$ , and  $P_2$ .

(c) For a given correlation time,  $P_2$  versus  $1/T_{1e}$  was plotted (see Fig. 3).

(d) The quantity  $R_2$ , equivalent to  $1/T_{2e}$  for a simple Lorentzian line, can be defined by rearranging Eq. 10:

$$R_2 = P_2[(\gamma_e \alpha)^2 T_{1e}]. \quad (13)$$

$R_2$  was computed for comparison with theory (Eqs. 3 and 11 and the Appendix).

Table 2 presents the results from the analysis:  $P_2$ ,  $\epsilon$ ,  $R_2$  for  $\sigma = 0.0$  G (no convolution) and  $R_w$  (measured from  $W$ ) given in Eq. 11. Table 3 shows results similar to Table 2 for spectra convolved with  $\sigma = 2.0$  G. Table 3 also contains additional information about the effects of inhomogeneous broadening (*vide infra*).

## RESULTS

Fig. 1 shows simulated lineshapes for two different correlation times. The top figure has  $\tau_c = 10$  ps (chosen for comparison with fast-motion theory), and the bottom one has  $\tau_c = 30$  ns (a correlation time typical of spectra obtained in the experiments of Altenbach et al. [10]). The signal height for analysis,  $\Delta Y$ , as well as the width at half-height,  $W$ , are indicated. The spectra show the signals well below saturation and have no convolution included; in an actual experiment the lines would be further broadened by unresolved protons or deuterons on the label. Clearly, as the correlation time increases, the spectrum does not remain as three sharp homogeneous lines.

Fig. 2 is a plot of signal height  $\Delta Y$  versus the incident microwave power  $P_0$  (the "rollover" saturation curve) for the spectra in Fig. 1.  $P_0$  was calculated from  $h_1$  as  $P_0 = (h_1/\alpha)^2$  and  $\alpha = 4.5$  G/ $\sqrt{\text{Watt}}$ , which is typical of a medical advances loop gap resonator (LGR);  $\alpha = 1.5$  G/ $\sqrt{\text{Watt}}$  for a standard TE<sub>102</sub> cavity (2). Eq. 12 is linearized with respect to  $c$  and  $P_2$  but requires a nonlinear search on  $\epsilon$ . This equation weights the low power terms more heavily to produce a reasonable fit, as can be judged from Fig. 2. The solid lines are the best least-squares fits to the  $\Delta Y$  predicted by Eq. 12 and the  $\Delta Y$  measurements from Fig. 1.

Fig. 3 shows a plot of  $P_2$  obtained from the rollover curves versus  $T_{1e}^{-1}$  for several fixed correlation times and  $T_{2e}^0$ . The values of  $T_{1e}$  were those entered into the simulation program in Table 2. Superimposed on the data is a least-squares best fit to the data of  $P_2 = \rho T_{1e}^{-1}$ , where  $\rho$  is an adjustable constant.

Fig. 4 shows the values of  $R_2$  as a function of  $\tau_c$  for different values of  $T_{1e}$  given in Table 2. In the curve on top in Fig. 4,  $T_{2e}^0 = 30$  ns, and on the bottom curve,  $T_{2e}^0 = 100$  ns. Also plotted is  $R_w$  given in Table 2, which is a rough estimate of  $R_{2e}$  for the low-field manifold obtained from the line's width at half height. Also shown on Fig. 4 are estimates of  $R_{2e}$  given by fast-motion relaxation theory (14), by a first-order modification to fast-motion

TABLE 2 Input parameters for simulations and parameters of rollover curve analysis

Input values			Results					
$\tau_c$	$T_{1e}$	$T_{2e}^0$	$\epsilon$	$P_2$	$R_2$	$T_2$	$W$	$R_w$
<i>s</i>	$\mu s$	<i>ns</i>		<i>mW</i>	<i>Mrad/s</i>	<i>ns</i>	<i>G</i>	<i>Mrad/s</i>
1E-11	0.25	30	1.465	21.3	33.41	29.9	1.55	33.02
1E-11*	0.25	100	1.489	6.33	9.94	100.6	0.405	9.96
1E-11	5	100	1.484	0.290	9.34	107.1	—	—
1E-9	0.25	30	1.34	26.9	42.15	23.7	—	—
1E-9	1	30	1.35	6.76	42.44	23.6	—	—
1E-9	5	30	1.302	1.25	39.31	25.4	2.321	46.6
1E-9	5	100	1.447	0.75	23.71	42.2	1.218	25.7
1E-8	0.25	30	1.224	92.7	145.4	6.87	—	—
1E-8	5	30	1.211	4.68	146.9	6.80	4.579	88.7
1E-8	5	100	1.224	4.27	134.2	7.45	3.522	68.6
3E-8	0.25	30	1.335	89.9	141.1	7.08	—	—
3E-8	1	30	1.325	24.4	153.4	6.51	—	—
3E-8	5	30	1.313	4.97	156.0	6.41	3.109	62.7
3E-8 <sup>‡</sup>	0.25	100	1.348	71.0	111.3	8.98	—	—
3E-8	1	100	1.42	19.8	124.3	8.04	—	—
3E-8	5	100	1.329	4.10	128.6	7.77	2.062	41.8
1E-7	5	30	1.384	5.03	157.9	6.33	—	—
1E-7	15	30	1.375	1.70	160.0	6.25	2.370	48.9
1E-7	5	100	1.418	3.94	123.8	8.07	—	—
1E-7	15	100	1.417	1.36	128.2	7.79	1.314	27.5
1E-5	5	30	1.137	1.58	49.76	20.09	1.858	34.8
1E-5	5	100	1.224	0.75	23.78	42.0	0.6036	11.7

Convolution = 0 G. See Table 1 for additional input parameters. The results of  $\epsilon$  and  $P_2$  are from fitting saturation rollover curves according to Eq. 13;  $R_2$  is calculated from Eq. 12.  $W$  is measured from the low power spectrum (see Fig. 1 for definition) and  $R_w$  is calculated from Eq. 11.

\* Set of calculations used for Figs. 1 and 2, *top*.

‡ Set of calculations used for Figs. 1 and 2, *bottom*.

theory (18), and by a generalized spectral density function suggested by multiple relaxation processes (see Appendix).

## DISCUSSION

Slowing of the rotational motion causes inhomogeneities due to the *g*- and *A*-tensors to become more pronounced (Fig. 1). The lineshape changes from a superposition of three homogeneous first-derivative Lorentzian shaped lines in the fast-motion limit to a complicated “powder pattern” spectrum at long correlation times. These changes in shape, especially in the center of the spectrum, cause the lines to overlap and make it difficult to estimate the height of the center line accurately. The peak height of the low field line is the best quantity to be used for a saturation rollover curve, as this place represents a spectral position that is easily identified at all motion times and is clearly associated only with a single line. This suggests that it would be better, experimentally, to use the an isotopically substituted <sup>15</sup>N nitroxide spin label rather than the <sup>14</sup>N analogue: there are only two EPR lines instead of three and the low field manifold of <sup>15</sup>N gives approximately two times bigger signal in the slow motion regime than does the <sup>14</sup>N label (19).

There is no simple a priori theory for the form of the rollover curve once one leaves the fast-motion regime. The use of Eq. 9 (or Eq. 12) to fit the rollover curve constitutes an approximation. These equations work remarkably well at fitting the results obtained directly from the simulations and continue to perform well even when Gaussian convolution is added. To obtain reliable estimates of  $\epsilon$  and  $P_2$  using Eq. 12, the rollover curves must be obtained over a large range of  $h_1$ : the rf field amplitude must be large enough to reduce the signal height at the highest rf field to 50% or less of the maximum. We note that such conditions in an actual experiment are difficult to obtain from commercial instruments without added heating and drift: the use of large volume (TE<sub>102</sub> or TM<sub>011</sub>) EPR cavities requires ~1 W of power incident on the resonator to produce a 1 G rf field. LGRs are more suitable for this work as they can produce 1 G of rf field at ~0.1 W incident power (2).

Consider now the dependence of  $\epsilon$  on the correlation time.  $\epsilon$  was chosen as an adjustable parameter because it varied depending on lineshape and degree of inhomogeneity. The hypothesis that  $\epsilon$  would be a valid monitor of the degree of inhomogeneity seems to be supported by the results (see Table 2). When the spectra consist of simple homogeneous first-derivative lines (i.e., fast-motion limit), then the rollover curves have an  $\epsilon = 1.49 \sim$

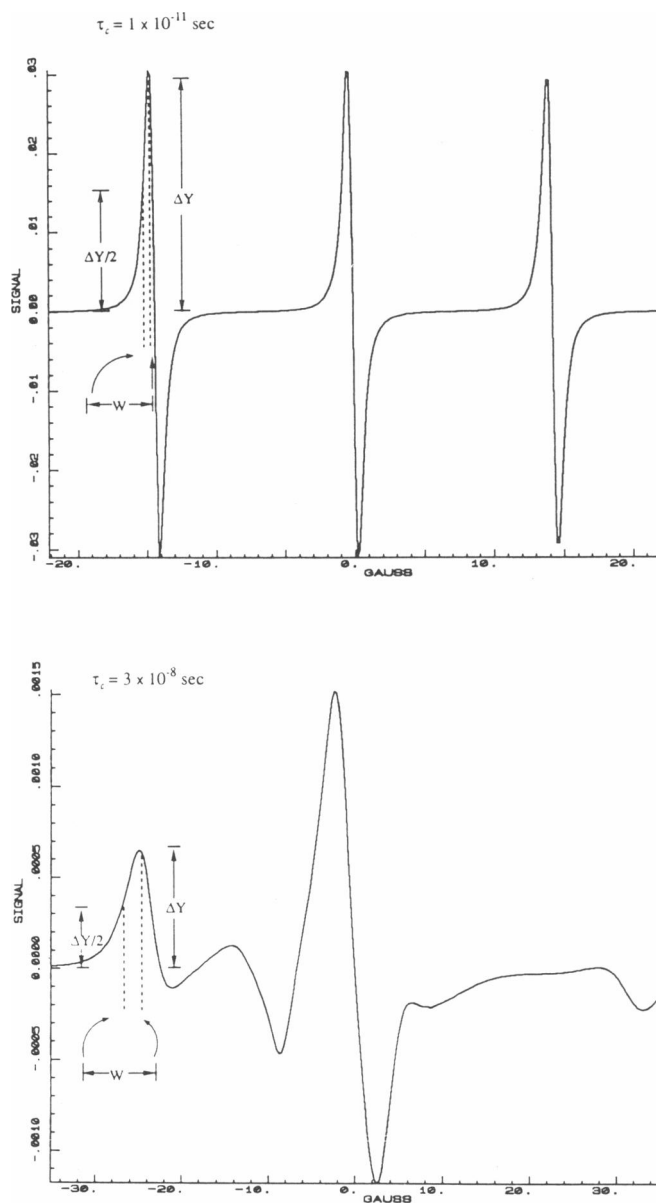


FIGURE 1 Simulated CW-EPR lineshapes for correlation times of  $\tau_c = 10^{-11}$  s (fast motion) and  $\tau_c = 3 \times 10^{-8}$  s (slow motion). The signal height for analysis,  $\Delta Y$ , is indicated on the spectra. Parameters used in the calculation were  $g_x = 2.0086$ ,  $g_y = 2.0066$ ,  $g_z = 2.0032$ ,  $A_x = A_y = 6.0$  G,  $A_z = 31.0$  G,  $T_{1e} = 1 \mu\text{s}$ ,  $T_{2e} = 30$  ns,  $h_1 = 0.04$  G.

$^{3/2}$ . As the motion slows, the value of  $\epsilon$  decreases as expected. When the motion is on the order of  $10 \mu\text{s}$   $\epsilon = 1.1$  to  $1.2 \sim 1.0$  (as expected for the low field turning point in a pure homogeneous absorption shape). The value of  $\epsilon$  at 30 ns motion is around 1.35 (still quite close to  $^{3/2}$ ). This value of  $\epsilon$  indicates that the line is still homogeneous at this correlation time even although the unsaturated CW-EPR spectrum has almost attained its rigid-limit lineshape.

In Fig. 3,  $P_2$  is shown as a function of  $T_{1e}^{-1}$ , with the motional rate and other parameters held fixed. The ex-

cellent agreement of the simple-proportionality model with the values of  $P_2$  strongly argues that  $P_2$  can be realized as a product of  $T_{1e}^{-1}$  and  $R_2$ , each of which is independent of the other. Again, there is no reason a priori that the  $P_2$  saturation rollover curve could be or should be interpretable in the simple fashion of Eq. 10; that it does we take as a fact based on our "computer experiments." This means that the rollover curve method of analysis allows one to extract values of  $T_{1e}$  under experimental conditions where  $R_2$  remains constant. The changes in  $T_{1e}$  are exactly reflected in changes in  $P_2$  (and qualitatively in  $P_{1/2}$ ).

This was the situation encountered by Altenbach et al. (10) in their study of  $P_{1/2}$  values from rollover curves. The spin labels on different residues all had  $R_2$ 's between 10 and 100 Mrad/s. The broad linear EPR linewidths in this motional range should not be very sensitive to low levels of oxygen, a local paramagnetic relaxing agent, but  $T_{1e}$  should be.  $T_{1e}$  does change markedly when a spin label attached to an amino acid side chain is either in contact with the relatively oxygen-poor environment of the protein interior or the relatively oxygen-rich lipid membrane. Altenbach et al. (10) assumed that  $P_{1/2}$  was

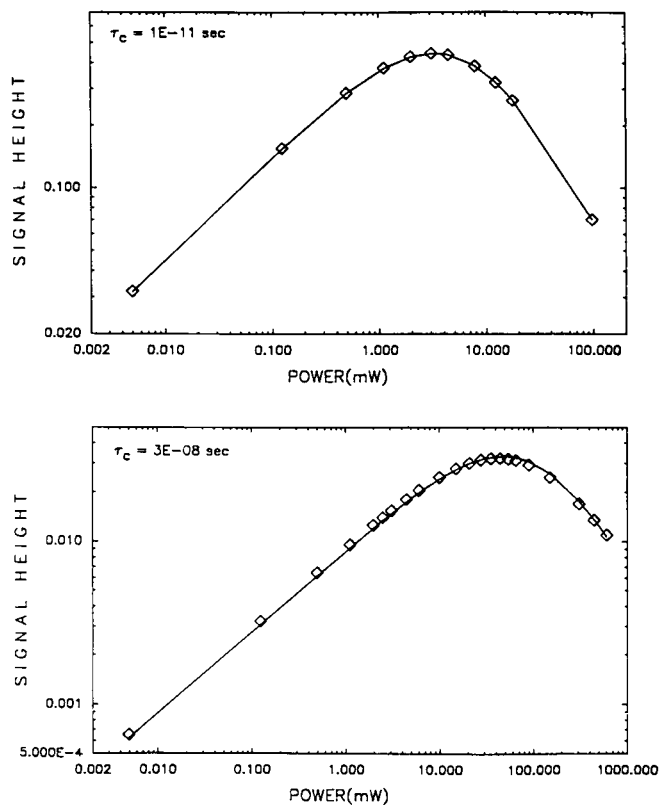


FIGURE 2 Plot of signal height  $\Delta Y$  versus the incident microwave power  $P_0$  (commonly called "rollover" saturation curves) for the two simulated spectra of Fig. 1: correlation times  $\tau_c = 10^{-11}$  s and  $\tau_c = 3 \times 10^{-8}$  s. The solid lines are the fits of the simulated lineshapes to the equation for signal height  $\Delta Y$  versus power  $P_0$  using Eq. 13. Fit parameters are given in Table 2.

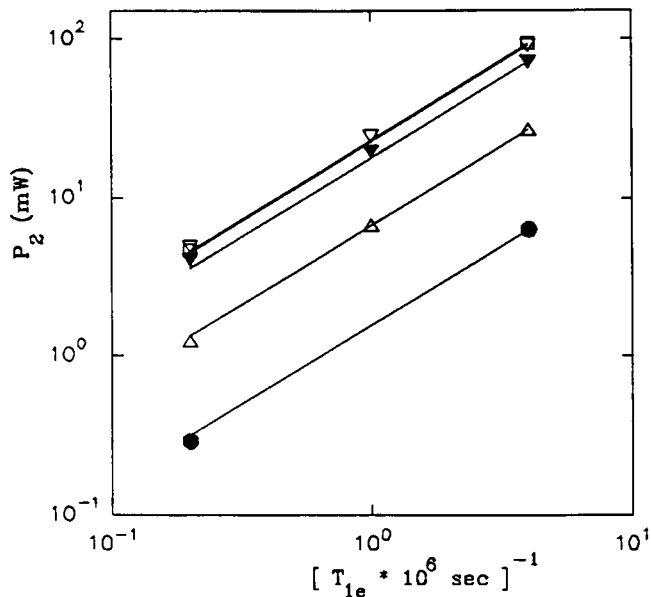


FIGURE 3 Plot of  $P_2$  obtained from the rollover curves like those of Fig. 2 versus  $1/T_{1e}$  for several correlation times. The values of  $T_{1e}$  were those entered into the simulation program. The various icons differentiate among  $P_2$  values calculated using the following input parameters:  $\tau_c = 10^{-11}$  s (circles);  $\tau_c = 10^{-9}$  s (triangles);  $\tau_c = 10^{-8}$  s (squares);  $\tau_c = 3 \times 10^{-8}$  s (inverted triangles). In addition, hollow icons indicate  $T_{2e}^0$  was 30 ns and filled icons indicate  $T_{2e}^0$  was 100 ns. The solid lines are the best fit straight lines to the data.

inversely proportional to  $T_{1e}$ . Our theory shows that this is so provided  $\epsilon$  does not change. At the correlation times used experimentally,  $\epsilon$  is approximately independent of  $T_{1e}$  (Table 2), so that their assumption was justified. In general, plots of  $P_{1/2}$  versus  $T_{1e}^{-1}$  would be slightly curved because, in fact,  $\epsilon$  is a weak function of  $T_{1e}$  (Table 2). This complicates the agreement between changes in  $P_{1/2}$  and changes in  $T_{1e}$ . However,  $P_{1/2}$  can be determined more easily than  $P_2$  from a rollover curve, and one is not required to go to large rf amplitudes; because  $\epsilon$  is not able to be found accurately, a direct conversion to a valid  $T_{1e}$  is not possible.

The rollover curves of Fig. 2 show that  $P_2$  (as well as  $P_{max}$ ) is dependent on  $\tau_c$  for fixed  $T_{1e}$ . In Fig. 2, the top curve ( $\tau_c = 0.01$  ns) is fit with  $P_2 = 6.3$  mW and the bottom one ( $\tau_c = 30$  ns) is fit with  $P_2 = 71.0$  mW,  $\sim 10$  times greater. This is because  $R_2$  is sensitive to  $\tau_c$ .

The success of Eq. 12 may be contrasted with the failure of Eq. 8 to relate  $L^2$  and  $P_0$ . Efforts to find a fitting function to linearize this relationship, that subsumed the effect of going from a derivative to an absorption shape, failed badly.

Fig. 4 shows the values of  $R_2$  as a function of  $\tau_c$  for different values of  $T_{1e}$  (see Table 2). In the top curve of Fig. 4,  $T_{2e}^0 = 30$  ns, and on the bottom curve,  $T_{2e}^0 = 100$  ns. The values of  $R_w$ , given in Table 2 and plotted on Fig. 4, provide a good estimate of  $R_2$  (equivalent to  $1/T_{2e}$ ) in

the fast-motion limit. Also plotted are estimates of  $R_{2e}$  ( $m$ ) from Eq. 4 for  $m = +1$  calculated from fast-motion theory given by Goldman (14) (long, dashed line), first-order modified fast-motion theory given by Hwang et al. (18) (short, dashed line), and a modified theory based on a generalized spectral density function (solid line; see Appendix).  $R_2$  at slow correlation times is a measure of the effective homogeneous linewidth under saturation. We would expect that  $R_2$  could not exceed a rate equivalent to the full linewidth of the low-field manifold,  $L_T$  (the distance between the  $z$  and  $y$  turning points). From Table 1 the value of  $L_T$  is 19.24 G (equal to 338 MRad/s as a rate). If the entire manifold were homogeneous with

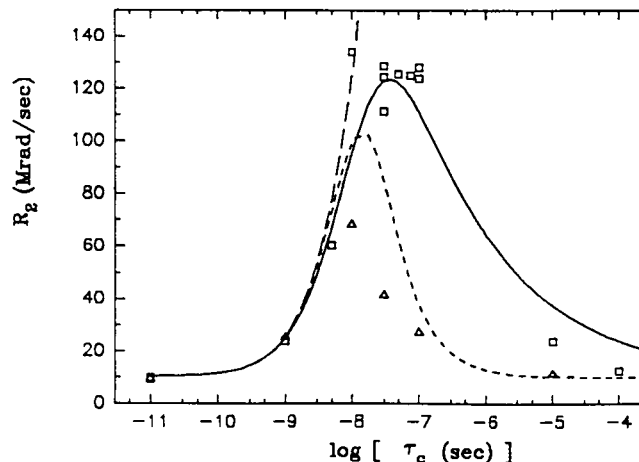
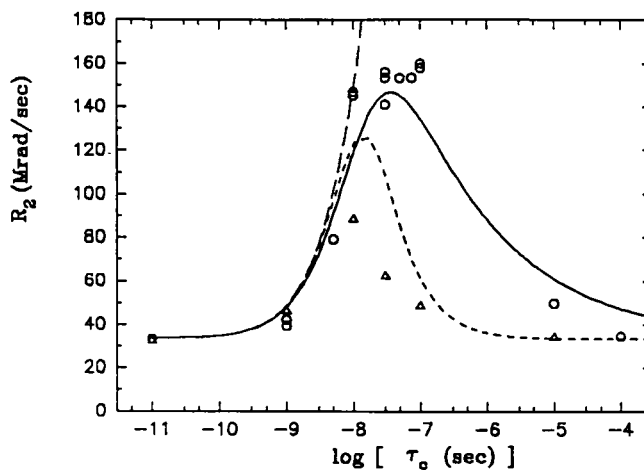


FIGURE 4 Plot of the value of  $R_2 \equiv P_2 [(\gamma_e \alpha)^2 T_{1e}]$  versus correlation time, taken from column 7 of Table 2. (Top)  $R_2$  (open circles) is plotted as a function of  $\tau_c$  for the case where  $T_{2e}^0 = 30$  ns and (Bottom) is the same as top except  $R_2$  is represented by open squares and  $T_{2e}^0 = 100$  ns. Also plotted is  $R_w$  (open triangles) (see Table 2) calculated from the measured linewidth, for comparison with  $R_2$ . The long dashed line is  $R_{2e}$  (Eq. 4 and Appendix) estimated by standard fast-motion theory ( $\kappa = 0, \beta = 2$ ). The short dashed line is  $R_{2e}$  from the Hwang et al. (18) modified fast-motion theory ( $\kappa = 1, \beta = 2$ ). The solid line is  $R_{2e}(m)$  calculated from the modified spectral density function with  $\kappa = 1.0$  and  $\beta = 1.3$  (See Appendix).

this value of  $L_T$ , then the effective  $R_2$  would be  $L_T/2$ . From Table 2 one can see that  $L_T/2 = 169$  Mrad/s is a very reasonable upper bound for  $R_2$ .

Both  $R_2$  and  $\epsilon$  are independent estimates of the extent of homogeneity of the EPR spectrum under conditions of saturation and both show that the lines appear to retain a large amount of homogeneous character even when the motion is slow (on the linear EPR timescale). Under such conditions, the (partially) saturated lineshapes are sensitive to  $T_{1e}$  as already discussed. A practical consequence of this is found in the slow-motion  $^{15}\text{N}$  spin-label study by Gaffney et al. (20). They observed broadening of the CW-EPR spectrum down to submicrosecond correlation times. We interpret this as an effect of saturation. As the motion slowed,  $T_{1e}$  lengthened so much so that the (fixed) observer power produced saturation. The slower the motion, the greater the degree of saturation, and hence the greater the line broadening (21).

We have established that a value of  $R_{2e}$  can be found from the simulations that enable one to calculate an accurate  $T_{1e}$ . It would be more satisfying to understand  $R_{2e}$  and how it varies with correlation time based on a more rigorous theory using spectral density functions. To illustrate the possible dependencies of  $R_{2e}$  (and  $R_2$ ) on motion, we present a single, general spectral density function estimate for  $R_{2e}$  that subsumes some specific cases considered by others:

$$R_{2e} = \delta^2 \frac{\tau_c}{1 + (\kappa \times \delta \times \tau_c)^\beta} + \frac{1}{T_{2e}^0}. \quad (14)$$

This form is consistent with fast-motion theory if  $\kappa = 0$  and  $\delta = [2/(3\sqrt{5})]\gamma_e L_T = 100$  Mrad/s. The modified fast-motion theory of Hwang et al. (18) has  $\kappa = 1$  and  $\beta = 2$ . (The full equations used for the calculations are given in the Appendix.)

Figure 4 shows that fast-motion theory values of  $R_{2e}$  ( $m = 1$ ) are always larger than  $R_2$  and those for the modified fast-motion theory are smaller than  $R_2$ . The modified fast-motion theory clearly avoids the (obviously incorrect) prediction that  $R_2$  grows without bound as the motion slows. Although  $R_{2e}$  ( $m = 1$ ) from the latter theory and  $R_w$  follow the same trend throughout the motional range, neither agrees well with  $R_2$  from the saturation curve.

We now consider how  $R_2$  is measured and why fast-motion theory cannot account for the observed values at correlation times slower than 5 ns.  $R_2$  is obtained under conditions of maximum saturation. As such, features of the EPR spectrum are responding nonlinearly to the observer power, and the linewidths of the individual packets are being broadened. On the timescale determined by  $T_{2e}$ , only correlation times out to 300 ns can be detected.  $T_{1e}$  being on the microsecond timescale allows very slow rotation of the spin label (correlation times as great as 10

TABLE 3 Input parameters for simulations and parameters of rollover curve analysis

Input values			Results					
$\tau_c$	$T_{1e}$	$T_{2e}^0$	$\epsilon$	$P_2$	$R_2$	$T_2$	$R_2^T$	$\sigma'$
s	$\mu\text{s}$	ns		mW	Mrad/s	ns	Mrad/s	G
1E-11	0.25	30	1.25	29.0	45.56	21.9	79.9	0.77
1E-9	5	30	1.255	1.81	56.85	17.6	83.7	1.03
1E-8	5	30	1.167	4.67	146.7	6.81	168.9	0.0
1E-8	5	100	1.167	4.34	136.2	7.34	157.8	0.0
1E-7	5	30	1.292	5.53	173.6	5.67	178.7	1.71

Convolution = 2 G. All parameters have the same meaning as in Table 2; however, all simulations were convolved with a 2-G Gaussian broadening function and then analyzed by the rollover curve method for  $P_2$  (and  $R_2$ ) and  $\epsilon$ , according to Eqs. 12 and 13.  $R_2^T$  was calculated from Eq. 16, where the Gaussian had  $\sigma = 2.0$  G = 35.2 Mrad/s.  $\sigma'$  was calculated from Eq. 17.

ms) to couple EPR resonance lines before the EPR signal decays (22).<sup>3</sup> The individual resonance lines are therefore in communication due to the motion on the timescale set by  $T_{1e}$ . In the slow-motion regime, at a fixed field-frequency position, there are many overlapping lines. In the absence of any motion, all lines relax with the same rate; when there is motion, the lines do not relax at the same rate because transfer of saturation competes with  $R_2$  relaxation. This leads to a clustering of different relaxation rates about a mean. The theory that treats such a situation suggests that  $R_2$  can be explained by the Cole-Davidson spectral density function in the frequency domain (or by a Williams-Watts stretched exponential function in the time domain) (23). The Cole-Davidson model has  $1 < \beta < 2$ , depending on the degree of spread of relaxation rates.

Consider how  $\beta$  depends on the correlation time and  $T_{1e}$ . When  $\tau_c$  is longer than  $T_{1e}$ , the flow of saturation between resonance lines ceases and  $\beta = 2$ . When the motion is faster than  $T_{1e}$ , the resonance lines are in communication, so  $\beta < 2$ . Conversely, if  $T_{1e}$  becomes smaller at a fixed correlation time, then  $\beta$  would become larger. Eq. 14 would therefore predict a slight decrease in  $R_2$  if  $T_{1e}$  were shorter. Table 2 shows that this prediction is correct: a 20-fold change in  $T_{1e}$  produces only a few percent change in  $R_2$ . Therefore, even in the very slow motion region,  $P_2$  can reasonably be interpreted as the product of  $R_2$  and  $T_{1e}^{-1}$ .

The effects of protons (or deuterons) on the EPR spectrum have been simulated by a convolution with a Gaussian function of width  $\sigma$ . Generally  $\sigma$  spans the range from 0.2 to 2.8 G. Several sets of calculated lineshapes were convoluted with a Gaussian ( $\sigma = 2$  G), and the saturation rollover curve of these spectra was analyzed

<sup>3</sup> See in particular Eq. 2.10 of Robinson et al (12).



according to Eq. 12. The results in Table 3 are rather surprising. The values of  $\epsilon$  decreased in all cases, as expected, removing some of the effect on  $R_2$  of the added inhomogeneity. Not all of the inhomogeneity was accounted for, and therefore the  $R_2$  ( $\sigma = 2$ ) was larger than the  $R_2$  ( $\sigma = 0$ ) for the corresponding set of lineshapes. Only for the spectra where  $\tau_c$  was about 10 ns did it happen that the decrease in  $\epsilon$  was just enough to keep  $R_2$  constant. One can be more quantitative by considering the expression given by Bales (16) for the effects of Gaussian convolution, adapted to our notation:

$$\left(\frac{\sqrt{3}\sigma}{R_2(\sigma)}\right)^2 + \left(\frac{R_2(0)}{R_2(\sigma)}\right) = 1. \quad (15)$$

This relation shows that the resulting linewidth,  $R_2(\sigma)$ , can be estimated if one has a Lorentzian line, characterized by  $R_2(0)$ , that is convoluted by a Gaussian of width  $\sigma$  to give a Voigtian lineshape. This relationship can be used to show how well the fitting function retrieves the original  $R_2(0)$ . Eq. 15 can be rearranged to solve for  $R_2$  ( $\sigma = 2$ ), called  $R_2^T$ , the total value one would expect if none of the convolution were removed:

$$R_2^T = R_2(0) \times \left\{ \frac{1 + \sqrt{1 + 12(\sigma/R_2(0))^2}}{2} \right\}. \quad (16)$$

$R_2^T$  (given in Table 3) would be expected to be an upper bound to  $R_2$ , and, presumably, if  $\epsilon$  did not change,  $R_2^T$  would equal the  $R_2$  extracted from the rollover fitting procedure. These expectations are borne out by the results in Table 3. Another way of viewing Eq. 15 is to rearrange it and solve for  $\sigma$ , called  $\sigma'$  (see Table 3), which is now an estimate of how much convolution was left behind after  $\epsilon$  was adjusted and the fitting was optimized:

$$\sigma' = \sqrt{\frac{R_2(\sigma) \times [R_2(\sigma) - R_2(0)]}{3}}. \quad (17)$$

$R_2(\sigma)$  is the  $R_2$  in Table 3 and  $R_2(0)$  is the  $R_2$  in Table 2 for the corresponding, nonconvoluted case. The conclusion is that when  $\tau_c$  is  $< 10$  ns,  $\sigma$  is reduced by about a factor of 2. Because the amount of convolution is small ( $\leq 0.5$  G) in this motional regime and half is removed, then the effects of Gaussian broadening are probably not going to affect estimates to  $P_2$  and  $R_2$ . However, when  $\tau_c$  is slower than 10 ns and the amount of broadening increases to around 2.8 G, considerable broadening remains. The results are clearly dependent on the motion. This finding is rather sobering for those who have used  $\epsilon$  in the past to remove the effects of inhomogeneous broadening.

## CONCLUSIONS

We have tested whether the simple idea of a saturation rollover curve, as given for a pure Lorentzian line, could be extended to estimate  $T_{1e}$  for nitroxide spin labels un-

dergoing motion. The first, and most fundamental, result is that Eq. 9 gives a remarkably good accounting of the simulated lineshapes (e.g., Fig. 2) when  $\epsilon$  is allowed to vary and be least-squares optimized. The second remarkable result is that  $P_2$  is very nearly proportional to  $T_{1e}^{-1}$ . These two results mean that the method can be used to obtain meaningful estimates of  $P_2$ . Changes in  $P_2$  reflect changes in  $T_{1e}$  under conditions where  $R_2$  remains constant. As modifications to the experimental protocol, we recommend measuring saturation on the low-field turning point and using Eqs. 9 or 12, with variable  $\epsilon$  to analyze the data. The method works well on the low-field line and does not work well on the center line. Measurements are made on the center line and analyzed but are not reported. Under some circumstances,  $\epsilon > 1.5$  was found! This occurred because the outer lines overlapped the center one, and this increases with increasing  $h_1$  due to broadening, raising the wings of the line to make it appear "super Lorentzian." Therefore, experimentally, one would be better off using the  $^{15}\text{N}$  isotopically substituted analogue for the nitroxide spin label. Moreover, because  $\epsilon$  does not remove Gaussian convolution very effectively, one is better off to use a fully perdeuterated  $^{15}\text{N}$  spin label with the narrowest possible linewidth for careful quantitative studies.

$T_{1e}^{-1}$  can be determined directly from spectral simulation: the  $A$ - and  $g$ -tensors, as well as  $T_{2e}^0$ ,  $\sigma$ , and the motional rate, are all determined from the linear CW-EPR lineshape.  $T_{1e}$  is only one unknown parameter remaining to be quantitatively determined from the rollover curve. Of course, rollover curves also can be simulated, using the programs that are derived from Eq. 1, varying  $T_{1e}$  until optimal agreement is found.

This process may be avoided by rearranging Eq. 13 for  $T_{1e}$ :

$$T_{1e}^{-1} = P_2(\gamma_e\alpha)^2/R_2. \quad (18)$$

Quantitative estimates of  $T_{1e}$  can be obtained using the values of  $P_2$ , determined from the experimental rollover curve, and  $R_2$ , generated by simulation or taken from Table 2. Methods for determining  $\alpha$  are described elsewhere (2). We have considered in detail the parameters that affect  $R_2$  and to what degree  $R_2$  is a valid description of the homogeneous linewidth under saturation.

We argue that  $R_2$  has validity in its own right, even though there is no simple a priori formula to determine it. The first point is that  $R_2$  is the same as that predicted by fast-motion theory in the regime where that theory is valid. The second point is that  $R_2$  is qualitatively described by the Hwang et al. (18) modified fast-motion theory over the entire motional range of interest. For example, at maximum  $R_2$ , modified fast-motion theory underestimates  $R_2$  by only  $\sim 20\%$ . The third point is that Table 2 and Fig. 4 demonstrate that  $R_2$  is a very weak function of  $T_{1e}^{-1}$ . The fourth and final point is that it is

plausible that the plateau of  $R_2$  between 10 and 200 ns may be accounted for by a motion-dependent  $\beta$ . Despite the limitations that have been pointed out in the discussion, Fig. 4 may be used to obtain a first-order estimate to  $R_2$ .

For rotational times faster than 5 ns,  $R_2$  may be estimated quite accurately from the fast-motion equations given in the Appendix. For rotational times from 10 to 200 ns,  $R_2$  is rather insensitive to motion. This then should be the optimal motional regime for obtaining  $T_{1e}$  by progressive saturation. For motions slower than a microsecond, ST-EPR spectra are directly sensitive to  $T_{1e}$  and can be directly compared (or simulated) to estimate  $T_{1e}$  (24).

We note that when  $\omega_m T_{1e} > 1.0$ , then the DC field modulation can affect the value of  $T_{1e}$  experimentally obtained (see Eq. 6). Based on direct measurements of  $T_{1e}$  with saturation recovery pulsed EPR (25), this condition is violated for motions slower than 0.1 ns when 100-kHz field modulation is used. It is therefore advisable that a modulation frequency much less than this be used in experiments with slower moving molecules.

## APPENDIX

The equation for  $R_{2e}^G(m)$  is given below. This was originally given in Goldman et al. (14) and later modified in Hwang et al. (18). It is further modified below to include a generalized spectral density function.

$$R_{2e}^G(m) = A(m) + mB(m) + m^2C(m),$$

where  $A(m)$ ,  $B(m)$ , and  $C(m)$  depend on  $m$ , which takes on the values  $m = 0, \pm 1$  for  $^{14}\text{N}$ . The following formulae are valid only for  $^{14}\text{N}$  where  $I = 1$ . These equations are identical to those in Goldman et al. (14) when  $\kappa = 0$  and  $\beta = 2$  and reduce to the  $A$ ,  $B$ , and  $C$  parameters defined therein and are identical to those in Hwang et al. (18) when  $\kappa = 1$  and  $\beta = 2$ .

$$\begin{aligned} A(m) &= \frac{I(I+1)}{5} \sum_{j=0}^2 \left(1 + \frac{j}{2}\right) (D_j)^2 \\ &\quad \times \left\{ \frac{1}{2} \left[ J_{j,\beta}(\omega_j^+(m)) + J_{j,\beta}(\omega_j^-(m)) \right] + \frac{7}{3} J_{j,2}(\omega_e) \right\} \\ &\quad + \frac{2}{5} \sum_{j=0}^2 \left(1 + \frac{j}{2}\right) (G_j)^2 \left\{ \frac{1}{3} J_{j,\beta}(\omega_3(m)) + \frac{1}{4} J_{j,2}(\omega_e) \right\}, \\ B(m) &= \frac{2}{5} \sum_{j=0}^2 \left(1 + \frac{j}{2}\right) (G_j D_j) \left\{ \frac{4}{3} J_{j,\beta}(\omega_3(m)) + J_{j,2}(\omega_e) \right\}, \\ C(m) &= \frac{1}{5} \sum_{j=0}^2 \left(1 + \frac{j}{2}\right) (D_j)^2 \\ &\quad \times \left\{ \frac{8}{3} J_{j,\beta}(\omega_3(m)) - J_{j,\beta}(\omega_j^m(m)) - \frac{1}{3} J_{j,2}(\omega_e) \right\}. \end{aligned}$$

The sum over  $j$  is only for  $j = 0$  and  $j = 2$ .  $C(m)$  is not defined, or needed, for  $m = 0$ . The generalized spectral density function is:

$$J_{j,\beta}(\omega) = \frac{\tau_j}{1 + (\omega\tau_j)^\beta},$$

and is valid for  $j = 0$  and 2 only.  $\tau_0 = 1/6d_\perp$  and  $\tau_2 = 1/(2d_\perp + 4d_\parallel)$ , where  $d_\parallel$  and  $d_\perp$  are the Einstein diffusion coefficients for rotation of an

axially symmetric object about its unique axis and perpendicular to the unique axis, respectively. These equations assume that the  $D$  (diffusion) and  $g$  and  $A$  tensors are all coincident.  $\omega_e = \gamma_e H_0$ , where  $\omega_e$  is the electron Larmor frequency and  $\omega_a = \gamma_e \bar{a}/2$ .

The other frequencies used constitute the various possible linear combinations associated with the manifold separations and widths:

$$\omega_j^\pm(m) = \left| \omega_a + (-1)^{(1+j/2)} \left[ \pm F_0 + (-1)^m \frac{D'}{2} \right] \frac{\kappa}{7} \right|,$$

and

$$\omega_3(m) = \left| \frac{2\kappa}{7} (F_0 + mD') \right|.$$

The elements of  $D$  and  $G$  are:

$$\begin{aligned} D_0 &= \frac{1}{\sqrt{6}} \gamma_e \left[ A_z - \frac{1}{2} (A_x + A_y) \right] \\ G_0 &= \frac{1}{\sqrt{6}} \omega_e \left[ g_z - \frac{1}{2} (g_x + g_y) \right], \\ D_2 &= \frac{1}{4} \gamma_e (A_x - A_y) \quad G_2 = \frac{1}{4} \omega_e [g_x - g_y], \\ D' &= \frac{2}{3} \gamma_e \left[ A_z - \frac{1}{2} (A_x + A_y) \right] \\ F_0 &= \frac{2}{3} \omega_e \left[ g_z - \frac{1}{2} (g_x + g_y) \right] / \bar{g}. \end{aligned}$$

$D_0$  and  $D_2$  are multiplied by  $2\pi$  as compared with  $D_0$  and  $D_2$  defined by Goldman et al. (14).  $G_0$  and  $G_2$  are multiplied by  $\omega_e/2$  as compared with the  $G_0$  and  $G_2$  defined by Goldman et al. (14).

To investigate how the generalized spectral density function of Eq. 14 could account for the observed values of  $R_2$ ,  $\kappa$  was set equal to one, various values of  $\beta$  were chosen, and the resultant  $R_{2e}$  curves were overlaid on the data. Having  $\beta < 2$  produces a broader maximum, but if  $\beta$  is set equal to unity,  $R_{2e}$  reaches a maximum and remains constant at longer  $\tau_c$ . No attempt was made to make  $\beta$  a function of  $\tau_c$  or  $T_{1e}$ , as would be necessary in a complete treatment. The estimate of  $R_{2e}^G(m)$  using  $\beta = 1.3$  (solid line, Fig. 4) shows that Eq. 14 can give a reasonable explanation of the dependence of  $R_{2e}^G(m)$  (and by implication  $R_2$  as well).

The authors acknowledge the support of the Natural Sciences and Research Council of Canada and the National Institutes of Health.

Received for publication 5 October 1992 and in final form 19 November 1992.

## REFERENCES

1. Poole, C. P. 1972. *Electron Spin Resonance: A Comprehensive Treatise on Experimental Techniques*. 2nd ed. Wiley, New York. 992 pp.
2. Mailer, C., D. A. Haas, E. J. Hustedt, J. G. Gladden, and B. H. Robinson. 1991. Low power EPR spin-echo spectroscopy. *J. Magn. Reson.* 91:475-496.
3. Czoch, R., and A. Francik. 1989. *Instrumental Effects in Homodyne Paramagnetic Resonance Spectrometers*. Ellis Horwood Ltd. New York. 395 pp.

4. Castner, T. G. 1959. Saturation of the Paramagnetic Resonance of an F-Center. *Phys. Rev.*, 115:1506.
5. Metz, H., G. Volkel, and W. Windsch. 1990. A Simple Method for Fitting of Inhomogeneous ESR Saturation Curves. *Phys. Status Solidi A*, 122:K73-K76.
6. Bowman, M. K., H. Hase, and L. Kevan. 1976. Saturation Behavior of Inhomogeneously Broadened EPR Lines Detected with Magnetic Field Modulation. *J. Magn. Reson.*, 22:23-32.
7. Clough, S., and C. A. Scott. 1968. Saturation and spectral diffusion in ESR. *J. Phys. Chem.* 1:919-931.
8. Freed, J. H., G. V. Bruno, and C. F. Polnaszek. 1971. ESR Line-shapes and Saturation in the Slow Motional Region. *J. Phys. Chem.* 75:3385-3399.
9. Freed, J. H. 1976. Theory of slow tumbling ESR spectra for nitroxides. In *Spin Labelling: Theory and Application*. Vol. I. L. J. Berliner, editor. Academic Press, New York. 53-132.
10. Altenbach, C., S. L. Flitsch, H. G. Khorana, and W. L. Hubbell. 1989. Structural Studies on Transmembrane Proteins 2. Spin Labelling of Bacteriorhodopsin Mutants at Unique Cysteines. *Biochemistry*. 28:7806-7812; and Altenbach, C., S. L. Flitsch, H. G. Khorana, and W. L. Hubbell. 1990. Transmembrane Protein Structure: Spin Labelling of Bacteriorhodopsin Mutants. *Science (Wash. DC)*. 248:1088-1092.
11. Dalton, L. R., B. H. Robinson, L. A. Dalton, and P. Coffey. 1976. Saturation Transfer Spectroscopy, *Advances in Magnetic Resonance*. Vol. 8. J. S. Waugh, editor. Academic Press, New York. 149-259.
12. Robinson, B. H., H. Thomann, A. H. Beth, P. Fajer, and L. R. Dalton. 1985. The phenomenon of magnetic resonance: Theoretical considerations. In *EPR and Advanced EPR Studies of Biological Systems*. L. R. Dalton, editor. CRC Press, Boca Raton, FL. 1-314.
13. Redfield, A. G. 1965. Theory of relaxation processes. In *Advances in Magnetic Resonance*. Vol. I. J. S. Waugh, editor. Academic Press, New York.
14. Goldman, A., G. V. Bruno, C. F. Polnaszek, and J. H. Freed. 1972. An ESR Study of Anisotropic Reorientation and Slow Tumbling in Liquid and Frozen Media. *J. Chem. Phys.* 56:716-735.
15. Beck, W. F., J. B. Innes, J. B. Lynch, and G. W. Brudvig. 1991. Electron Spin-Lattice Relaxation and Spectral Diffusion Measurements on Tyrosine Radicals in Proteins. *J. Magn. Reson.* 91:12-29.
16. Bales, B. 1989. Inhomogeneously broadened spin-label spectra. In *Biological Magnetic Resonance*. Vol. 8.—Spin Labeling: Theory and Applications. L. J. Berliner and J. Reuben, editors. Plenum Press, New York.
17. Beth, A. H., K. Balasubramanian, B. H. Robinson, L. R. Dalton, and S. D. Park. 1983. Sensitivity of ST-EPR Signals to Anisotropic Diffusion with <sup>15</sup>N Nitroxide Spin Labels. Effects of Non-coincident Magnetic and Diffusion Tensor Principal Axes. *J. Phys. Chem.* 87:359-367.
18. Hwang, J. S., R. Mason, L. P. Hwang, and J. H. Freed. 1975. ESR Studies of Anisotropic Rotational Reorientation and Slow Tumbling in Liquid and Frozen Media. III. Perdeuterated 2,2,6,6-Tetramethyl-4-piperidone N-Oxide and an Analysis of Fluctuating Torques. *J. Phys. Chem.* 79:489-511.
19. Beth, A. H., and B. H. Robinson. 1989. Nitrogen-15 and deuterium substituted spin labels for studies of very slow motional dynamics. In *Spin Labeling: Theory and Applications. Biological Magnetic Resonance*. Vol. 8.—Spin Labeling: Theory and Applications. L. J. Berliner and J. Reuben, editors. Plenum Press, New York. 179-253.
20. Gaffney, B. J., C. H. Elbrecht, and J. P. A. Scibilia. 1981. "Enhanced Sensitivity to Slow Motions using <sup>15</sup>N-Nitroxide Spin Labels," *J. Magn. Reson.* 44:436-446.
21. Robinson, B. H., and L. R. Dalton. 1979. "EPR and Saturation Transfer EPR Spectra at High Microwave Field Intensities," *Chem. Phys.* 36:207-237.
22. McConnell, H. M. 1975. Molecular motion in biological membranes. In *Spin Labeling: Theory and Applications*. Vol. I. L. J. Berliner, editor. New York. 525-561.
23. Lindsay, C. P., and G. D. Patterson. 1980. "Detailed Comparison of the Williams-Watts and Cole-Davidson Functions," *J. Chem. Phys.* 73:3348-3357.
24. Robinson, B. H. 1983. "Effects of Over-Modulation on Saturation Transfer EPR Signals," *J. Chem. Phys.* 78:2268-2273.
25. Mailer, C., B. H. Robinson, and D. A. Haas. 1992. "New Developments in Pulsed EPR. Relaxation Mechanisms of Nitroxide Spin Labels," *Bull. Magn. Reson.* 14:30-35.